Anisotropic low-energy vibrational modes as an effect of cage geometry in the binary barium silicon clathrate Ba$_{24}$Si$_{100}$

Romain Viennois,[1,*] Michael Marek Koza,[2] Régis Debord [ORCID],[3] Pierre Toulemonde,[4] Hannu Mutka [ORCID],[2] and Stéphane Pailhès[3,†]

[1]*ICGM, Université Montpellier, CNRS, Ecole Nationale Supérieure de Chimie de Montpellier, Montpellier, France*
[2]*Institut Laue Langevin, 71 avenue des Martyrs, F-38042 Grenoble, France*
[3]*Institute of Light and Matter, UMR5306 Université Lyon 1-CNRS, Université de Lyon 69622 Villeurbanne cedex, France*
[4]*Université Grenoble Alpes, CNRS, Grenoble INP, Institut Néel, F-38000 Grenoble, France*

The low lattice thermal conductivity in inorganic clathrates has been shown recently to be related to the low-energy range of optical phonons dominated by motions of guest atoms trapped in a network of host covalent cages. A promising route to further reduce the heat conduction, and increase the material efficiency for thermoelectric heat waste conversion, is then to lower the energy of these guest-weighted optical phonons. In the present work, the effect of the host cage geometry is explored. The lattice dynamics of the binary type-IX clathrate, Ba$_{24}$Si$_{100}$, has been investigated experimentally by means of inelastic neutron scattering as a function of temperature between 5 and 280 K, and computed by *ab initio* density functional techniques. It is compared with the lattice dynamics of Ba$_8$Si$_{46}$, the simplest representative of the well-known type-I clathrate structure. The binary Ba$_8$Si$_{46}$ and Ba$_{24}$Si$_{100}$ materials have both a cubic unit cell made of different Si cages. The energies, the degree of anharmonicity as well as the anisotropy of the optical phonon modes weighted by Ba motions are found to depend strongly on the size and shape of the cages. The lowest optical phonon energies in Ba$_{24}$Si$_{100}$ are found around 2.5–4 meV, while those in Ba$_8$Si$_{46}$ have higher energies around 7–9 meV. The low-lying optical phonons in Ba$_{24}$Si$_{100}$ are mainly weighted by the motion of Ba in the opened Si$_{20}$ cage, which does not exist in Ba$_8$Si$_{46}$. Moreover, the Ba vibrations within the opened Si$_{20}$ cages are found intrinsically anisotropic, strongly dispersionless in some directions, and exhibit a significant anharmonicity, which is not observed for any optical phonon modes in Ba$_8$Si$_{46}$.

I. INTRODUCTION

Clathrates are representatives of "guest-host" structures and form a wide class of inorganic materials whose crystal structure results in a three-dimensional (3D) covalent framework of face-sharing polyhedral cages encapsulating guest cations. Their peculiar crystalline structure offers the possibility of tuning their electronic properties between metallic, semiconducting and even superconducting for some compositions. Concomitantly, they exhibit a very low thermal conductivity of as low as $1-2\,\mathrm{W\,m^{-1}\,K^{-1}}$ at room temperature approximating values found in glassy materials. The conjunction of low electrical resistivity and low thermal conduction are making them promising candidate materials for thermoelectric (TE) applications [1–6].

In clathrates, especially for compositions optimized for TE applications, the heat transport is dominated by lattice thermal conductivity (λ_L), described microscopically by quasiparticles called phonons. Despite their low thermal conductivity, inelastic x-ray and neutron spectroscopies reveal the existence of well-defined acoustic phonons [6–11]. They are efficient heat carriers propagating their energies with an average sound velocity of about $3\,000\,\mathrm{m\,s^{-1}}$ over distances of a few tens of nanometers, which correspond to several unit cells ($\sim$1 nm) of the type-I clathrate crystals [11]. However, their energies are typically restricted to a range of less than 10 meV ($\sim$100 K). Indeed, at higher energies, the phonon spectrum consists of nearly nondispersive optical phonon branches, which "cut through" the acoustic branches [6–12]. The low-lying optical bands are dominated by vibrations of the guests in the cages [2]. In the case of the most studied type-I clathrate structure, whose simplest representative is the binary Ba$_8$Si$_{46}$, the low-lying optical branches are prevailed by motions of Ba in tetrakaidecahedra Si$_{24}$ cages. These Ba-weighted optical modes are viewed as well-defined peaks in the phonon density of states (DOS) [13–18] and lead to a broad hump in the temperature dependence of the specific heat (C_p) over the T^3 Debye dependence [16,19–23]. Recently, a universal relation has been revealed in type-I clathrates between λ_L and the product of the average sound velocity by the hump temperature in $C_p(T)$ [23]. This hump temperature is commonly associated in literature to an Einstein temperature (θ_E) and corresponds in the phonon spectrum to the lowest optical guest phonon energy (E_1) such that $E_1 = k_B\theta_E$. In the context of the Boltzmann transport equation for phonons, the propagative acoustic component of the lattice thermal conductivity is given by the following spectral integral whose upper limit is

---

*Corresponding author: romain.viennois@umontpellier.fr
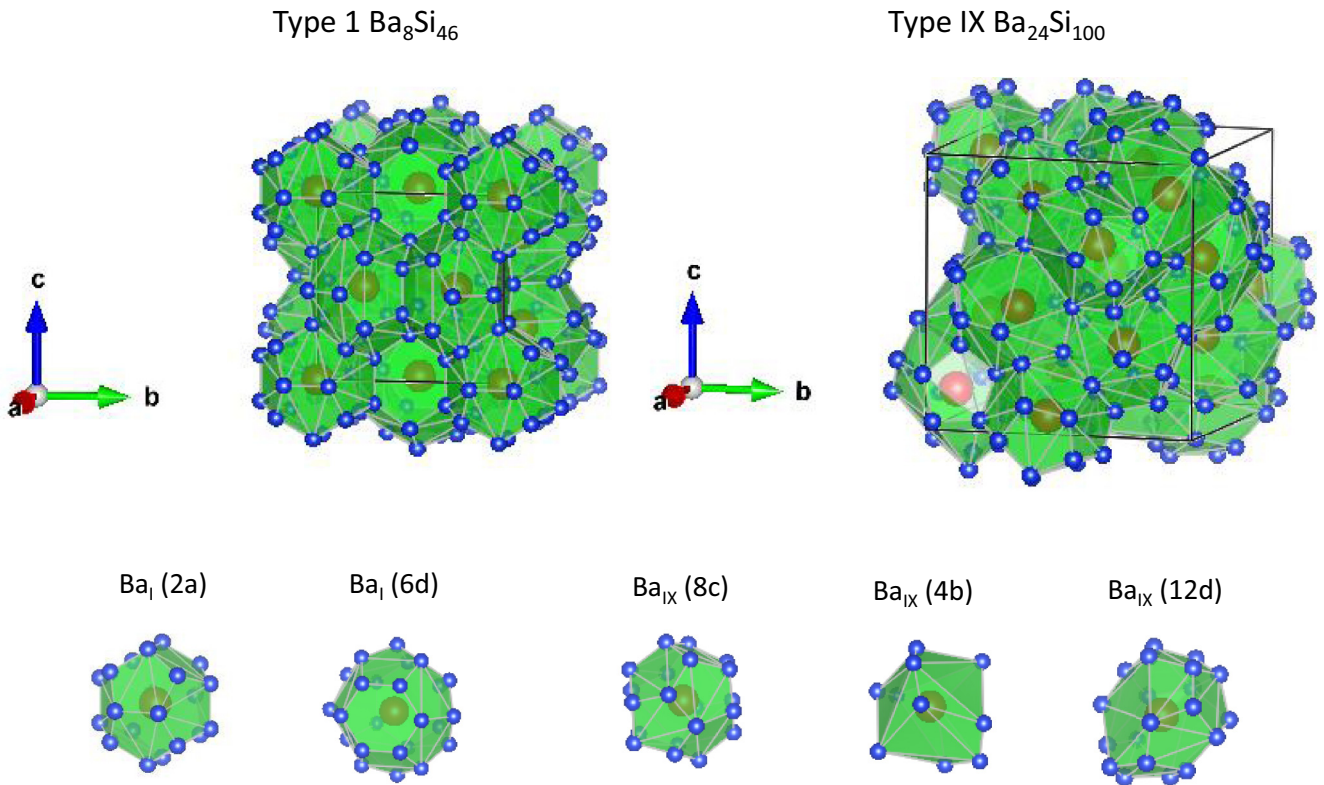†Corresponding author: stephane.pailhes@univ-lyon1.fr

Type 1 Ba$_8$Si$_{46}$

Type IX Ba$_{24}$Si$_{100}$

Ba$_I$ (2a)   Ba$_I$ (6d)   Ba$_{IX}$ (8c)   Ba$_{IX}$ (4b)   Ba$_{IX}$ (12d)

FIG. 1. Crystal structures of type-I clathrate Ba$_8$Si$_{46}$ (a) and of type-IX clathrate Ba$_{24}$Si$_{100}$ (b) plotted using the Vesta software [31]. The top row displays the Si (blue spheres) polyhedra (light green) centered by Ba atoms (red spheres) in the cubic unit cell (black line). In the bottom row, the building units of each clathrate structures are shown: type-I clathrate is made of Si$_{20}$ ($V \sim 104.9$ Å^3) and Si$_{24}$ ($V \sim 148.5$ Å^3) polyhedra occupied by Ba$_I$(2a) and Ba$_I$(6d), type-IX clathate is made of closed ($V \sim 68.2$ Å^3) and open Si$_{20}$ ($V \sim 102.2$ Å^3), Si$_8$/Si$_{11}$ ($V \sim 99.5$ Å^3) polyhedra occupied by Ba$_{IX}$(8c), Ba$_{IX}$(12d) and Ba$_{IX}$(4b) atoms, respectively.

locked by E_1 [6–11,23]:

$$\lambda_L(T) = \int_0^{E_1} \lambda_L(E)\rho(E)dE, \qquad (1)$$

where $\lambda_L(E)$ is the thermal conductivity of acoustic phonons with energies in the range $E + dE$ and $\rho(E)$ is the density of states.

Thus, lowering the energy E_1 of the guest optical phonons reduces efficiently λ_L. The nature of the low-lying guest optical phonons is particularly intriguing. *Ab initio* calculations in the harmonic approximation in type-I clathrates demonstrate that the sole complexity of the 3D framework of cages cannot explain the low value of λ_L so that the guest vibrations have a particular role [24]. It has been found that these guest optical phonons exhibit very low participation ratios (PR) [9,10,25–28]. Furthermore, perturbative *ab initio* calculations in type-I clathrates show that the existence of nearly nondispersive optical phonon branches results in a strong enhancement of the phonon-phonon scattering which contribute to lower the lattice thermal conductivity [24,25,29]. An efficient route to reduce λ_L in clathrates is then to lower the energies of low-lying guest modes. This can be done in type-I clathrates by the substitution of host atoms or the creation of vacancies in the host framework which, by deforming the host cage, can not only smoothen the guest potential but also split the centered guest equilibrium positions into off-centered minima in the cages [2,30].

An alternative route, which is explored in this work, is to investigate the effect of the cage geometry in the binary clathrate of type-IX, Ba$_{24}$Si$_{100}$. The cubic crystal structure of Ba$_8$Si$_{46}$ (space group Pm-$3n$) and Ba$_{24}$Si$_{100}$ (space group $P4_132$) are shown in the Figs. 1(a) and 1(b), respectively. The lattice parameter in the type-IX, of about 14 Å, is much higher than the one of the type-I, of about 10.5 Å. The type-I unit cell consists of six large tetrakaidecahedra $5^{12}6^2$ Si$_{24}$ cages and two small pentagonal dodecahedra 5^{12} Si$_{20}$ cages, which encapsulate two different barium sites, the Ba$_I$(6d) and Ba$_I$(2a), respectively. The type-IX unit cell, shown in Fig. 1(b), is composed of eight Si$_{20}$ dodecahedra, four Si$_8$ distorted cubes, and 12 Si$_{20}$ open cages leading to three different sites for the barium atoms, namely Ba$_{IX}$(8c), Ba$_{IX}$(4b) and Ba$_{IX}$(12d), respectively [32–35]. The type-I clathrate is composed of sp^3 Si atoms only while, in the type-IX, Si atoms of the distorted Si$_8$ cubic cavity have both sp^3 and sp^2 bond characters [32–35].

In this paper, we investigate the phonon dynamics in Ba$_{24}$Si$_{100}$ mostly in the energy range of the low-lying dispersionless modes. Combining INS and *ab initio* density functional theory (DFT) calculations, our study reveals the existence of an additional guest optical band around 2.5–4 meV in Ba$_{24}$Si$_{100}$, which is not present in Ba$_8$Si$_{46}$. In general, the DFT results back up the existence of low-energy optical modes in Ba$_{24}$Si$_{100}$ and show that they are mostly weighted by Ba displacements in the Si$_{20}$ dodecahedra cages. Moreover,

the calculations reveal that these modes are characterized by very low values of the PR similar to the ones of the lowest-lying guest phonons in the type-I clathrate. In addition, while the guest potential is nearly harmonic in Ba_8Si_{46} [10,24], a significant deviation from harmonicity is found in $Ba_{24}Si_{100}$.

II. EXPERIMENTAL AND COMPUTATIONAL DETAILS

The $Ba_{24}Si_{100}$ samples were synthesized under high pressure and high temperature conditions in a large volume press with "Conac"-type anvils at the CNRS, Grenoble, France. A mixture of Si and $BaSi_2$ powders in stoichiometric amounts were loaded in a boron nitride crucible within a graphite furnace and were submitted to a pressure of about 1.1 GPa followed by heating to 650 °C for 1 hr. The samples were then thermally quenched and the pressure was slowly decreased. More details can be found in Refs. [33] and [36]. Our samples contain some amount of secondary phases such as diamond silicon (10–15%) and cubic $BaSi_2$ (3%), however, they are insignificant for the conclusions of this study as confirmed by the comparison with the DFT calculation results.

High-resolution inelastic neutron scattering (INS) experiments were performed with the IN5 time-of-flight spectrometer [37] at the Institut Laue Langevin in Grenoble, France. Some preliminary results obtained from previous experiments with the time-of-flight spectrometers IN4 and IN5 in a low-resolution configuration were reported in Refs. [16] and [38]. The experiments with higher resolution and improved signal permit us to discriminate different low-energy features in the INS spectra. More importantly, our experimental configuration allowed us to study the temperature dependence of the lowest energy modes. We have used different incident wavelengths, however, most of the results reported here were obtained with a wavelength of 3 Å resulting in an elastic energy resolution of about 0.3 meV. The generalized density of states (GDOS) $G^{exp}(\omega, T)$ was computed within the incoherent approximation similarly to a recent approach performed for skutterudites [39–41]. For the investigation of the temperature dependence of the vibrational spectrum a standard cryostat with a He atmosphere of about 10 mbars at 100 K was used.

Lattice dynamics calculations were carried out with the direct method from the Hellmann-Feynman (HF) forces computed on the relaxed clathrate structures with the Vienna *ab initio* software package (VASP). The HF forces were derived by displacing atoms from their equilibrium positions by 0.05 Å along nonequivalent high-symmetry directions. The DFT calculation was based on projector augmented plane-wave pseudopotentials and the Perdew-Burke-Ernzerhof (PBE) exchange-correlation functional [42,43]. We have used the finite-temperature smearing first order Methfessel-Paxton method for the band occupancies [44]. For all calculations an energy cut-off of 320 eV and the energy convergence of 10^{-6} eV was applied. We applied k meshes of $5 \times 5 \times 5$ and $9 \times 9 \times 9$ for $Ba_{24}Si_{100}$ and Ba_8Si_{46}, respectively. The relaxed lattice parameters found are 14.15 Å for $Ba_{24}Si_{100}$ and 10.39 Å for Ba_8Si_{46}. They are slightly larger than the experimental values by about 0.6–0.7% (14.06–14.07 Å for $Ba_{24}Si_{100}$ [33,34,36], 10.32–10.33 Å for Ba_8Si_{46} [36,45]) which is typical for a PBE exchange correlation functional [46].

TABLE I. Characteristic energy and potential parameters of Ba guests in type-IX (top) and type-I (bottom) Ba-Si clathrates derived from DFT results. K_2, K_3, and K_4 are harmonic and anharmonic potential parameters from the fitting of Ba potentials with the polynomial function $y = K_2\Delta x^2 + K_3\Delta x^3 + K_4\Delta x^4$. E_2 corresponds to the characteristic energy calculated from K_2, and the dimensionless anharmonic parameter β is computed from the quartic force constant K_4 according to the DUM [68].

Guest atom	K_2 (eV/Å^2)	K_3 (eV/Å^3)	K_4 (eV/Å^4)	E_2 (meV)	β
Ba_{IX}(8c)	2.48	−0.23	0.98	8.7	0.005
Ba_{IX}(4b)	1.26		0.81	6.2	0.013
Ba_{IX}(12d) [100]	0.33	−0.00	0.11	3.2	0.013
Ba_{IX}(12d) [001]	1.41	−0.33	0.97	6.5	0.013
Ba_I(2a)	2.62		0.84	8.9	0.004
Ba_I(6d) [100]	1.29		0.47	6.3	0.007
Ba_I(6d) [010]	1.02		0.20	5.6	0.004

The lattice dynamics properties and neutron spectra were computed from the HF forces by the diagonalization of the dynamical matrix with the software package Phonon [47]. For the calculations of the phonon DOS, 20 000 q points were sampled using the Monte-Carlo technique. For a better comparison of the experimental $G^{exp}(\omega, T)$ with the DFT results, powder average lattice dynamics (PALD) calculations were performed to derive the equivalent $G^{PALD}(\omega, T)$ and using 372000 q points. More details on the computational procedure are given in Refs. [39,48,49]. The atomic displacement parameters have been computed using the software package PHONON [47] and as described by Ref. [49]. The PR $p(\omega)$ of the phonons describes the degree of participation of the different atoms to a particular vibrational mode [9,10]. It has been extracted from the above calculations using [9,10]

$$p(\omega) = \left(\sum_{i=1}^{N} |\vec{u}_i(\omega_{\vec{q}})|^2 \right)^2 \Big/ N \sum_{i=1}^{N} |\vec{u}_i(\omega_{\vec{q}})|^4, \qquad (2)$$

where $\vec{u}_i = \vec{e}_i(\vec{q})/\sqrt{M_i}$ are the atomic amplitudes with the phonon polarization vector $\vec{e}_i(\vec{q})$ and the mass M_i of atom i.

III. RESULTS

The *ab initio* potential energy landscapes (ΔE) probed by Ba atoms in the various cages in type-I and type-IX clathrates have been computed from small displacements Δx out of the equilibrium position (see Supplemental Material) [50] and reported in Fig. 2 along the guest site high-symmetry directions [100] and [010] in type-I clathrate and [100] and [001] in type-IX clathrate, respectively. We report the ΔE of Si atoms in type-IX clathrate in the Supplemental Material [50]. Polynomial fits, $\Delta E(\Delta x) = K_2\Delta x^2 + K_3\Delta x^3 + K_4\Delta x^4$, have been performed in order to quantify and compare the deviations from the harmonic potential. The harmonic K_2, and the anharmonic cubic K_3 and quartic K_4 terms are reported in Table I. Note that due to the lower symmetry of the Ba_{IX}(8c) and Ba_{IX}(12d) sites, the cubic terms K_3 are nonzero for any direction and along [001], respectively. In any Si cage of the two clathrate types, the potential energy curves take on

minimum values at $\Delta x = 0$ so that the guest equilibrium positions are at the center of the cages. In both cases, the amplitude of the harmonic term K_2 is much lower for Ba than for Si, which is the result of the weaker bonds between Ba-Si than Si-Si. In type-I clathrates, the smallest K_2 values are found for $Ba_I(6d)$ located in the large Si_{24} cage. Due to the asymmetry of the Si_{24} cage (see Fig. 1), the $Ba_I(6d)$-Si distance varies from 3.5 Å, in the equatorial plane of the cage [parallel to the *bc* plane in the inset of the Fig. 2(d)], to 3.825 Å along the [100] sixfold symmetry axis. The in-plane $Ba_I(6d)$ potential is the smoothest with the lowest K_2. As a result, optical phonon branches weighted by in-plane $Ba_I(6d)$ modes have the lowest energies [51–53]. In $Ba_{24}Si_{100}$, the smallest K_2 is found for the out-of-plane $Ba_{IX}(12d)$ potential in the Si_{20} open cage [along the [100] twofold symmetry axis and parallel to the *bc* plane in the inset of the Fig. 2(c)]. Its value is about three times lower than the one of the in-plane $Ba_I(6d)$ potential Moreover, the Ba motion within the Si_{20} open cage, with $Ba_{IX}(12d)$-Si distance varying from 3.27 to 4.222 Å, is more anisotropic than in the Si_{24} cage. The largest cage dimension is along the twofold axis, i.e., in the direction of the smoothest K_2. This anisotropy difference is best visible when comparing guest potentials along and perpendicular to the high symmetry axes (parallel to the [100] direction) in

the open Si_{20} and Si_{24} cages as shown in Fig. 2. In addition, the potential energy of Ba atoms in the type-IX clathrate, especially that of $Ba_{IX}(12d)$, exhibits significant deviations from harmonicity, as illustrated in Fig. 2 where the harmonic (dotted blue points) and anharmonic (red lines) curves are superimposed. On the other hand, no significantly anharmonic term is needed to approximate the $Ba_I(6d)$ potential in the same range of displacements.

The smoother out-of-plane $Ba_{IX}(12d)$ potential compared to the in-plane $Ba_I(6d)$ potential agrees with the observation of larger Ba atomic displacement parameters (ADPs) in $Ba_{24}Si_{100}$ than in Ba_8Si_{46} as reported by Toulemonde *et al.* [34] and by Fukuoka *et al.* [54]. Our *ab initio* calculations of the ADPs for the different Ba sites corroborate qualitatively these experimental findings (see Supplemental Material) [50]. The highest ADP value obtained for $Ba_{IX}(12d)$, of about 0.03 Å^2, is almost two times larger than the one obtained for $Ba_I(6d)$, of about 0.017 Å^2. The in-plane versus out-of-plane anisotropy of the Ba potential in the Si_{24} and Si_{20} cages is also clearly visible in the *ab initio* derived ADPs shown in Figs. 2(c) and 2(d), respectively. The large anisotropy of the ADPs for $Ba_{IX}(12d)$ has been already reported experimentally in the type-IX clathrates $Ba_{24}Ge_{100}$ [35,55–58] as well as for $K_{IX}(12d)$ in $K_{24}Sn_{100}$ [59]. Its origin is intrinsic to the asym-
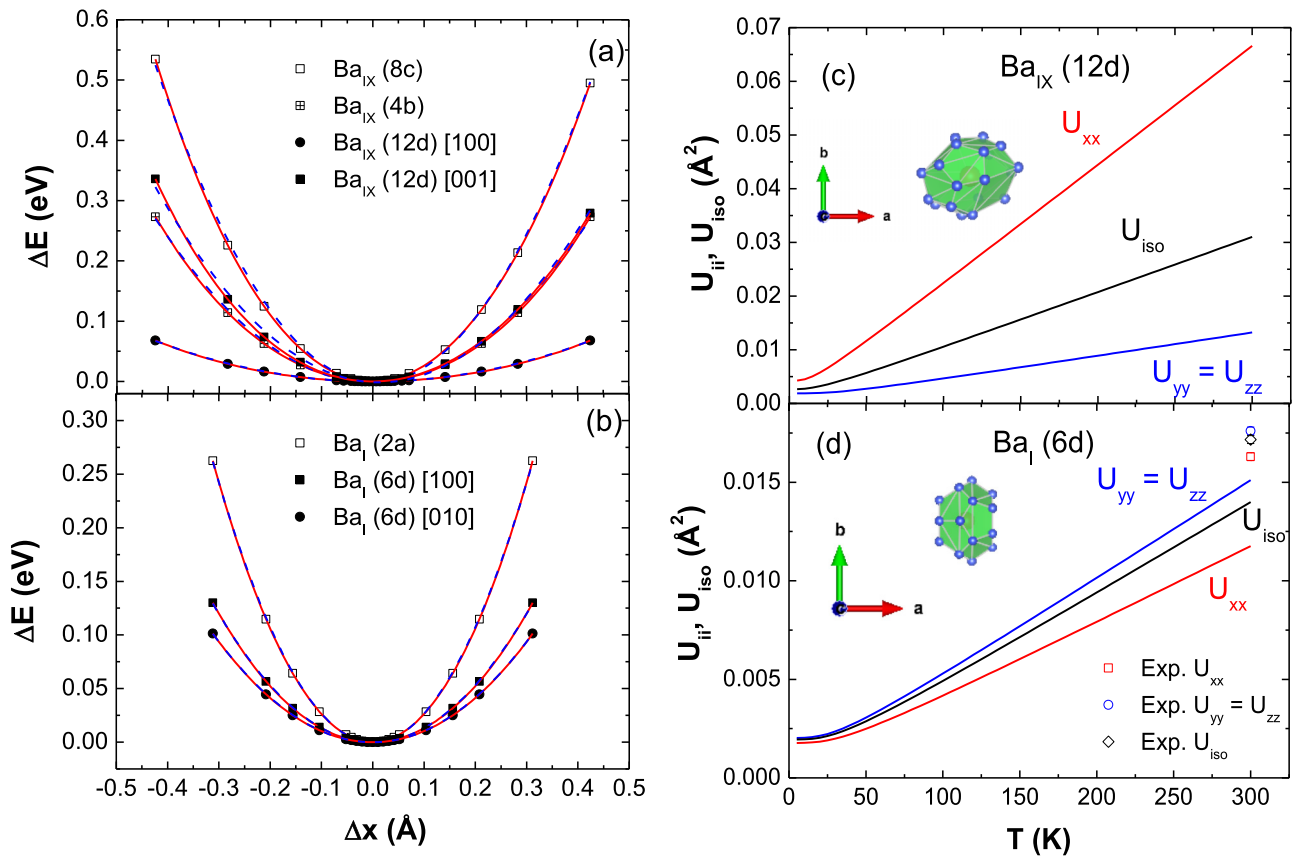

FIG. 2. (Left column) *Ab initio* calculated atomic potential ΔE vs Δx displacement of the Ba atoms in $Ba_{24}Si_{100}$ (a) and Ba_8Si_{46} (b). The red solid lines represent results from a polynomial fit up to fourth order. Blue dotted lines represent fit results with a harmonic, squared potential. (Right column) Temperature dependence of the diagonal U_{ii} and isotropic U_{iso} atomic displacement parameters of $Ba_{IX}(12d)$ in open Si_{20} cages of $Ba_{24}Si_{100}$ (c) and of $Ba_I(6d)$ in Si_{24} cages of Ba_8Si_{46} (d). Lines correspond to DFT derived results and open symbols with $Ba_I(6d)$ in Ba_8Si_{46} to experimental data [54]. The insets in (c) and (d) show an open Si_{20} cage of $Ba_{24}Si_{100}$ projected in the *ab* plane and an Si_{24} cages of Ba_8Si_{46} projected in the *ab* plane, respectively.
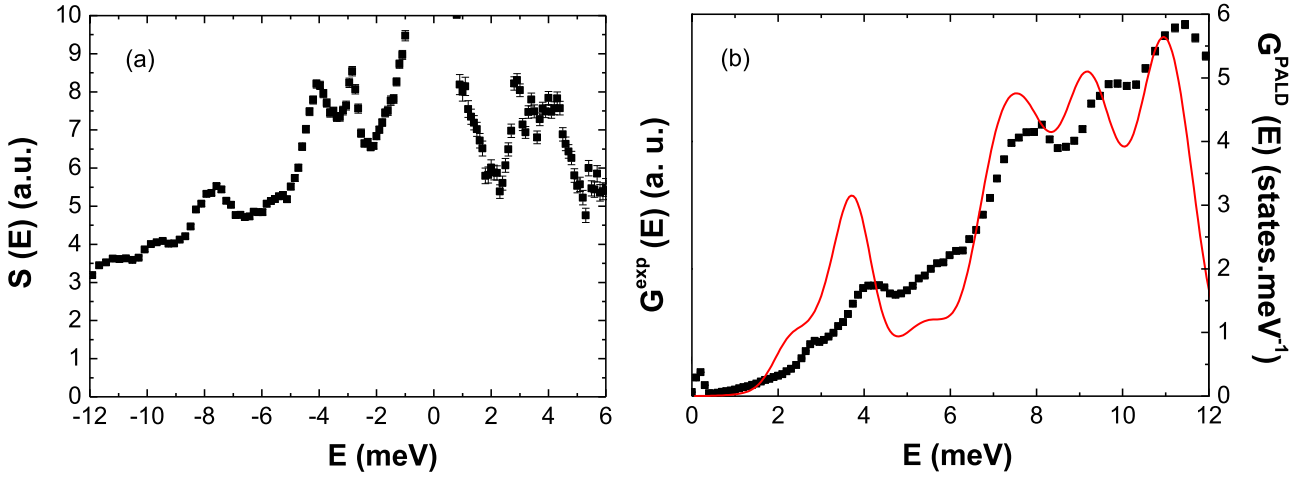
FIG. 3. Inelastic response of the type-IX clathrate $Ba_{24}Si_{100}$ measured by INS in the low-energy range of Ba-dominated modes. (a) Dynamic structure factor $S(E, T = 280\,K)$, (b) generalized density of states $G^{exp}(E, T = 280\,K)$ obtained from INS experiments (solid symbols) compared to the powder averaged lattice dynamics computed density of states $G^{PALD}(E, T = 280\,K)$.

metric shape of the open X_{20} cages [60]. On the other hand, the *ab initio* computed ADPs are almost isotropic for $Ba_{IX}(8c)$ and $Ba_{IX}(4b)$ in $Ba_{24}Si_{100}$ and for $Ba_I(2a)$ in Ba_8Si_{46} in agreement with experiments (see Supplemental Material) [50].

The dynamical structure factor, $S(E)$, recorded at 280 K in $Ba_{24}Si_{100}$ by means of neutron time-of-flight spectroscopy (see experimental and computational details) and the GDOS, $G^{exp}(E)$, which can be computed from $S(E)$ [50], are shown in Figs. 3(a) and 3(b) only in the low-energy range from 0 to 12 meV. The higher energy range is shown in the Supplemental Material [50].

The $G^{exp}(E)$ of $Ba_{24}Si_{100}$ has been measured at several temperatures in the range 5–280 K, as reported in Fig. 4(a) in the Debye representation, i.e., $G^{exp}(E)/E^2$. Owing to the improved instrumental resolution regarding our previous measurements reported in Refs. [16,38], we identify three additional low-energy peaks centered at energies of

$E_1 = 2.8$, $E_2 = 3.5$, and $E_3 = 4$ meV at 280 K. Our *ab initio* calculation of the phonon DOS is shown in Fig. 5(a) in the 0–12 meV energy range. In the energy range above 12 meV, our *ab initio* calculations reported in the Supplemental Material [50] agree with the previous report [61]. Furthermore, the phonon DOS is better resolved in our calculations thanks to a larger sampling of the reciprocal space. A powder-averaged phonon DOS, $G^{PALD}(E)$, has been reconstructed from the *ab initio* data (see experimental and computational details) and compared directly to the experimental $G^{exp}(E)$ as shown in Fig. 3(b). The $G^{PALD}(E)$ reproduces the low-energy features at $E_{1,2,3}$ observed in $G^{exp}(E)$ with a slight energy difference of about 10%. In previous works [62,63], we reported a similar difference in energy between *ab initio* derived and the experimental Raman active phonon energies. The calculated phonon dispersions along the high symmetry directions in $Ba_{24}Si_{100}$ and the total phonon density of states are shown in
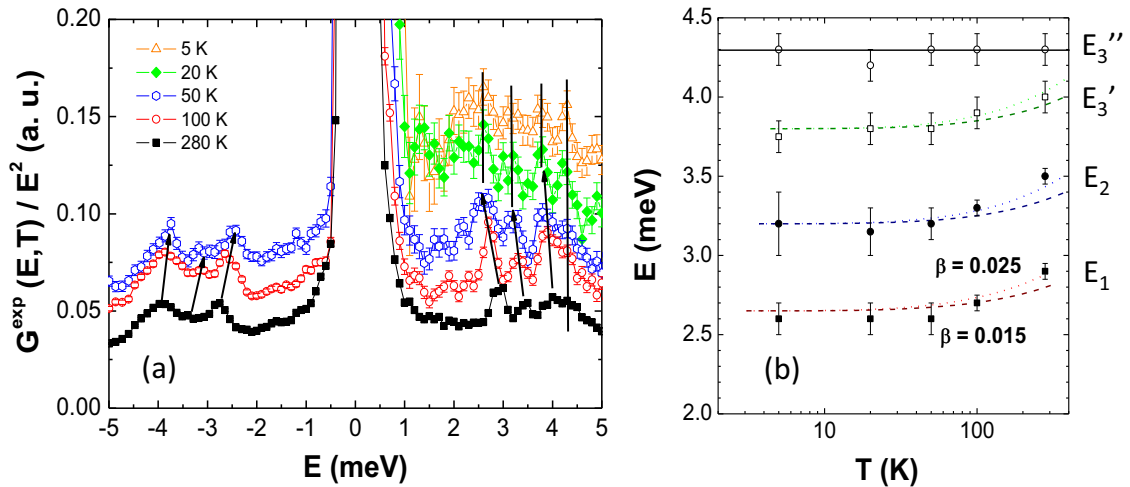

FIG. 4. (a) Temperature dependence of $G^{exp}(E, T)/E^2$ of $Ba_{24}Si_{100}$. Temperatures are listed in the figure. Right and left sides correspond to the Stokes and anti-Stokes lines, respectively. Arrows are guides for the eye indicating the peak shift upon cooling. (b) Temperature dependence of the peak energies identified and fitted in $G^{exp}(E, T)/E^2$. Lines correspond to calculations with the DUM [68] characterizing the anharmonicity of the fitted peaks by a dimensionless parameter β whose value is 0.015 for dashed lines and 0.025 for dotted lines.
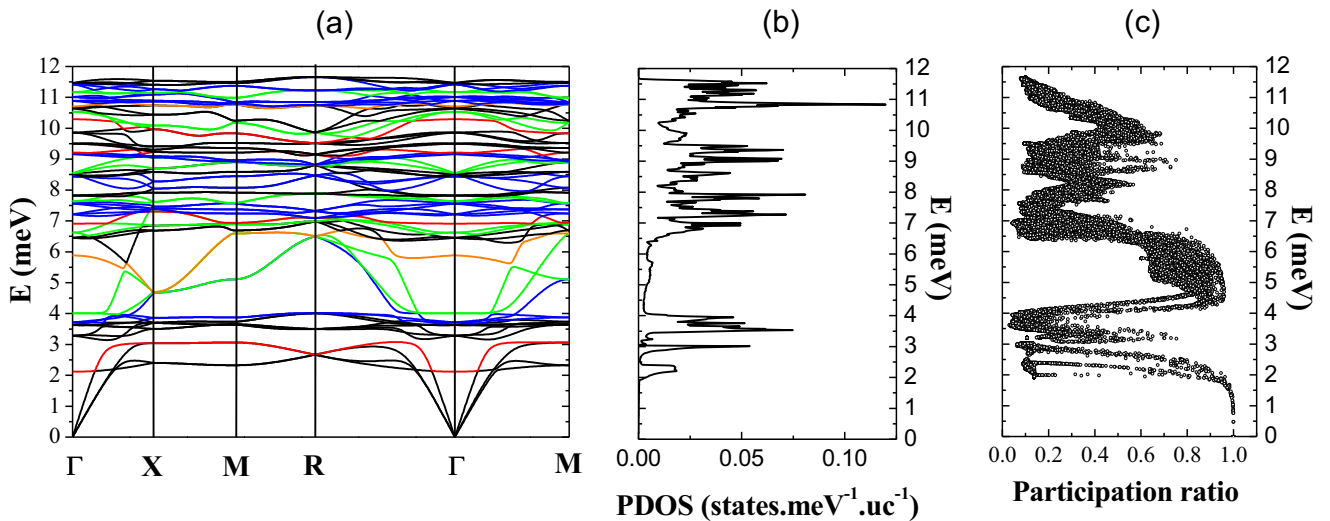
FIG. 5. Phonon dispersion curves (a), phonon density of states (PDOS) (b) and phonon participation ratio (c) calculated for the type-IX $Ba_{24}Si_{100}$ clathrate in the energy range 0–12 meV. The phonon dispersion curves have been computed along the high symmetry directions in the Brillouin zone. The color code with the dispersion curves indicates the symmetry of the modes at the Γ point: A_1 (orange), A_2 (red), E (green), T_1 (black), T_2 (blue).

Figs. 5(a) and 5(b), respectively, whereas the partial phonon DOS (p-DOS) for each atom is depicted in Fig. 6(a).

Based on this set of theoretical data, the experimental peaks $E_{1,2,3}$ can be assigned to some specific atomic vibrations. The peak at E_1 is ascribed not only to the optical branch of A_2 symmetry (optically silent mode) whose calculated energy at Γ is 2.1 meV but also to the bending and extensive nondispersive character of the low-energy transverse acoustic (TA1) branch in the vicinity of the Brillouin zone boundary.

The peak at E_2 is associated in an analogous way with the bending and extensive nondispersive character of the high-energy transverse and longitudinal acoustic branches (TA2 and LA, respectively) in the vicinity of the Brillouin zone boundary and to the sum of optical branches with T_1 symmetry (infrared active) with energies of about 3.3 meV at the Γ point.

The peak at E_3 is interpreted as the sum of optical branches with T_1 and T_2 symmetry (Raman active) with energies of about 3.6, 3.7, and 4 meV at the Γ point. The $E_{1,2,3}$ optical bands are mostly dominated by $Ba_{IX}(12d)$ vibrations in the open Si_{20} cages as seen in the phonon p-DOS in Fig. 6(a). The lowest-lying optical branch corresponds to out-of-plane vibrations of the $Ba_{IX}(12d)$, i.e., along the twofold symmetry axis, in open Si_{20} cages as evidenced in the directional p-DOS, whereas the in-plane $Ba_{IX}(12d)$ weighted optical phonons perpendicular to this axis are found at higher energies between 5 and 12 meV [see Fig. 6(b)]. This anisotropy is a consequence of the Si_{20} cage geometry as discussed above. The optical phonon branches associated with $Ba_{IX}(8c)$ and $Ba_{IX}(4b)$ vibrations occupy as well the energy range between 5 and 12 meV [see Fig. 6(a)].

The existence of optical phonons with very low energies around 3 meV in $Ba_{24}Si_{100}$ was formerly considered in the
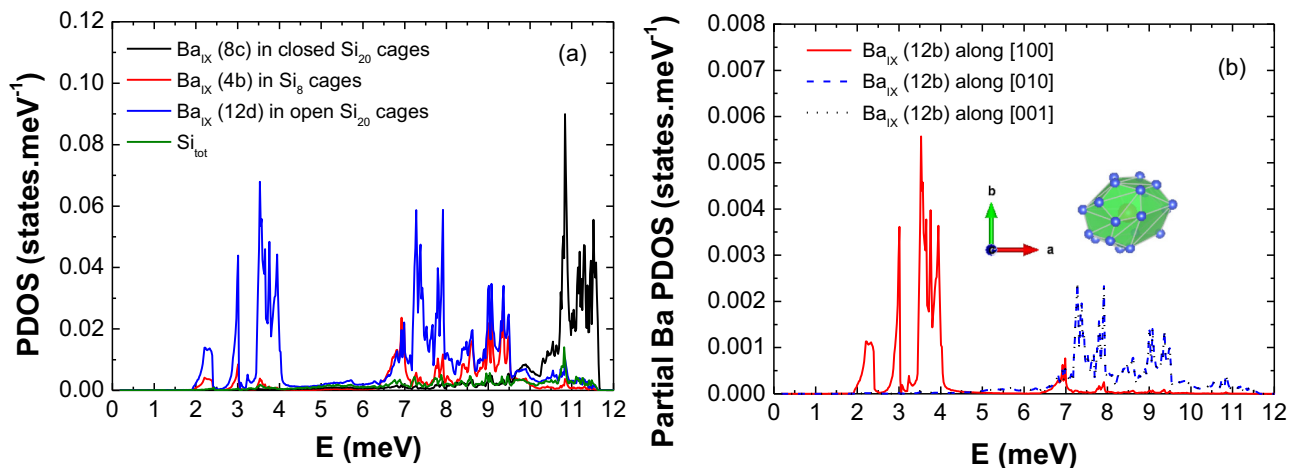

FIG. 6. (a) Partial phonon density of states (p-DOS) for the different Ba atoms and for all the Si atoms; (b) partial phonon density of states for the $Ba_{IX}(12d)$ atoms projected along the high symmetry direction (here [100]) and the other directions (here [010] and [001]) calculated for the type-IX $Ba_{24}Si_{100}$ clathrate in the energy range 0–12 meV.
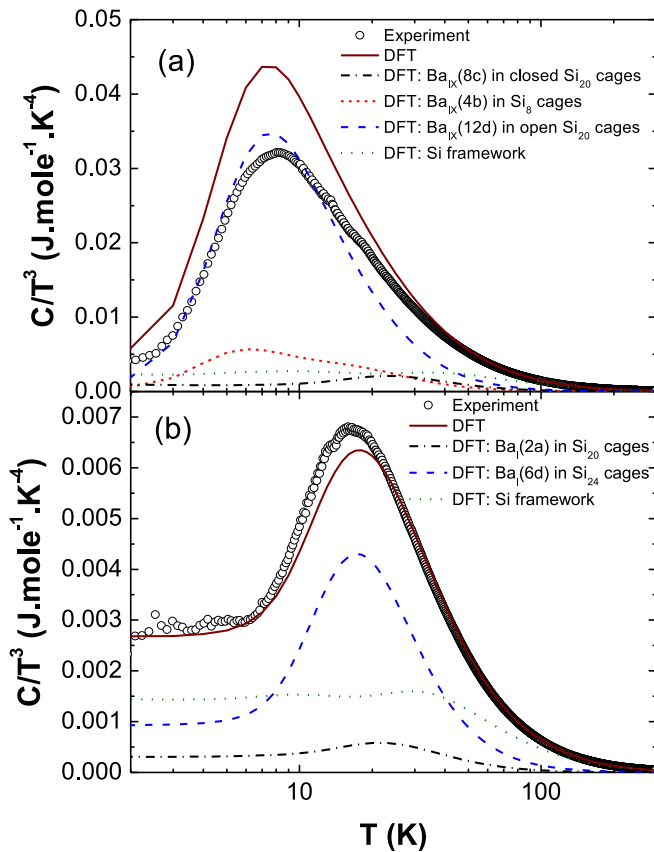
FIG. 7. Total and partial heat capacity $C_v(T)$ derived from DFT calculations plotted in a Debye plot C/T^3 vs T and compared to experimental data $C_p(T)$ [16] for $Ba_{24}Si_{100}$ (a) and Ba_8Si_{46} (b).

analysis of the C_p of $Ba_{24}Si_{100}$ [16]. The experimental [16] and calculated temperature dependences of the lattice heat capacity, shown in the Debye representation (C_p/T^3 versus T), in $Ba_{24}Si_{100}$ and in Ba_8Si_{46} are reported in the Fig. 7. As commonly observed in all clathrates, the temperature dependence of C_p/T^3 deviates significantly from the Debye behavior and forms a broad peak whose temperature of its maximum is related to the energy of the low-lying optical modes. The temperature of this peak in $Ba_{24}Si_{100}$ of about 8 K is clearly lower than in Ba_8Si_{46} of about 15 K and thus consistent with the energy downshift of the optical phonons in $Ba_{24}Si_{100}$ in comparison with those in Ba_8Si_{46}. In order to disentangle the atomic contributions to the peak in C_p/T^3, we have computed from the *ab initio* derived phonon spectrum the heat capacity from each atomic site in both clathrates, see Fig. 7. It shows that the peak in C_p/T^3 is dominated by vibrations of $Ba_{IX}(12d)$ in $Ba_{24}Si_{100}$ and by vibrations of $Ba_I(6d)$ in Ba_8Si_{46}.

The phonon PR, which can be interpreted as the relative number of atoms participating to a particular eigenstate with an essentially nonzero amplitude can be well taken as a measure for the modes localization behavior. Propagating acoustic modes comprise eigenstates with PRs close to unity as they are characterized by a long wavelength in-phase displacement of all atoms. Localized optic modes, on the other hand, comprise eigenstates with a substantial number of zero or antiphase atomic displacements, which show a highly dis-

persed amplitude distribution for a compound with distinctly different atomic masses. In this case and for complex crystal structures, where the optical branches are very flat, the PRs in the optical regime can take on values lower than 0.1. We report in Fig. 5(c) the energy-projected phonon PR in $Ba_{24}Si_{100}$. As expected, in the acoustic limit corresponding to energies lower than about 1.8 meV the PR takes on values of unity. It decreases abruptly when eigenstates with zero and antiphase amplitudes become prominent. Eigenstates with minimum values of less than 0.04 are observed in the energy range of the low-dispersive modes forming the E_3 peak. Recent theoretical works using DFT in type-I clathrates have related these low PRs values to an effect of phonon localization [24,29].

Now, we discuss the temperature dependence of the low-energy $E_{1,2,3}$ peaks of the generalized density of states that is reported in Fig. 4(b). The E_1 and E_2 peaks exhibit a significant softening, of about 0.3–0.5 meV, i.e., about 10–15%, upon cooling down to 5 K. The E_3 peak, viewed as a unique and broad distribution of modes at 280 K, splits in two peaks which are separated by about 0.5 meV at the base temperature. They are labeled E_3' and E_3'' with $E_3' < E_3''$. The energy of the E_3' peak decreases upon cooling while that of the E_3'' peak remains almost unchanged in the sampled temperature range. The thermal shift of the mode energies results from the sum of a first term due to the thermal expansion of the unit cell and a second isochoric term caused by the anharmonicity change which, to the first order in perturbation, is given by the quartic component in the potential energy [64,65]. The thermal expansion energy shift (ΔE^{TE}) is given by the product of the mode energy (E) by the lattice thermal expansion (α) and the Grüneisen parameter (γ): $\Delta E^{TE} = -\alpha\gamma\Delta T$. The Grüneisen parameter for the low-lying optical modes in $Ba_{24}Si_{100}$ and Ba_8Si_{46} have been found positive and of about $+2$ and the values of their thermal expansion are in the $10^{-5}\,K^{-1}$ range [16,66]. Thus, the change in energy due to the thermal expansion is positive upon cooling and counts for about 2.5% of the mode energy, i.e., less than 0.1 meV in the case of $Ba_{24}Si_{100}$. On the contrary, we observed a softening of the $E_{1,2,3}$ with the decrease of the temperature with an amplitude of about ~ 0.3 meV, which cannot be ascribed to the effect of the lattice thermal expansion. In $A_8Ga_{16}X_{30}$ (A = Sr, Ba, Eu and X = Ge,Sn) [2,8,51–53,67] a similar softening of the $Ba_I(6d)$-weighted optical phonons was observed, however, by only 0.1–0.2 meV and thus weaker than in $Ba_{24}Si_{100}$. It was interpreted that the mode softening upon cooling is a signature of an appreciable contribution of the quartic and higher terms of the bonding potential to the mode anharmonicity [29]. The simple model of the anharmonic isolated oscillator, derived by Dahm and Ueda (DUM) [68], is commonly used to compare the strength of the anharmonicity among different materials. In this approach, the renormalization of the eigen-energy of the harmonic oscillator, E, is given by the anharmonic quartic term K_4 whose amplitude is expressed by the dimensionless parameter β : $\beta = 4K_4\hbar^4/E^3M^2$ [68]. This parameter can be extracted from the measurement of the temperature dependence of E. The DUM model has been used to fit the temperature dependence of the peaks E_1, E_2, E_3' and E_3'' as reported in Fig. 4(b). Due to the uncertainties in the peak definition, only a range of values for β of 0.015–0.025 can be approximated for E_1, E_2, E_3'. β is almost null for

the peak E_3''. The strength of the quartic term in $Ba_{24}Si_{100}$ is about one order of magnitude lower than in other cage-based systems known as being highly anharmonic, such as the pyrochlore KOs_2O_6 with $\beta \sim 0.7$ [69], the tetrahedrite $Cu_{12}Sb_2Te_2S_{13}$ with $\beta \sim 0.1$–0.5 [70] and MV_2Al_{20} ($M =$ Al and Ga) with $\beta \sim 2 - 20$ [71]. On the other hand, the range of values for β found in $Ba_{24}Si_{100}$ is slightly higher than the one observed in some other cage-based materials where anharmonicity is assumed to play an important role in the thermal conduction such as in type-I $Ba_8Ga_{16}Ge_{30}$ ($\beta = 0.014$) [51], in Cs-osmate pyrochlore ($\beta = 0.025$) [69] and in the skutterudite $YbFe_4Sb_{12}$ ($\beta = 0.013$) [72]. Thus, if $Ba_{24}Si_{100}$ can be considered mostly as being harmonic, the anharmonic term of the $Ba_{IX}(12d)$ potential is higher than the one of the $Ba_I(6d)$ potential. This corroborates with the deviation of the *ab initio* potentials from the quadratic behavior observed for $Ba_{IX}(12d)$ and not for $Ba_I(6d)$, see Fig. 2. As another consequence of the anharmonicity the phonon energies found in experiment at the base temperature are closer to the computed DFT results than the ones observed at room temperature. The harmonic energies, $E_2 = (K_2/M)^{1/2}$, as well as the anharmonicity parameters, β, can be simply estimated from polynomial fits to the *ab initio* Ba potentials. Along the (100) direction in $Ba_{24}Si_{100}$, an harmonic energy of 3.3 meV is obtained for $Ba_{IX}(12d)$, which matches very well with the peak energy in the directional phonon p-DOS [see Fig. 6(b)]. This agreement is another signature of the localized character of the $Ba_{IX}(12d)$-weighted phonons. The values of β as extracted from the *ab initio* $Ba_{IX}(12d)$ potential lies in the 0.013–0.014 range depending on the direction that is very close to that obtained experimentally. It is then interesting to notice that, in the case of $Ba_{24}Si_{100}$, the quartic term can be extracted from the calculated potentials in the harmonic approximation. On the other hand, in Ba_8Si_{46}, an harmonic energy of 6.3 meV is extracted from the $Ba_I(6c)$ potential along the [100] direction while, in the phonon DOS, the corresponding peak is located at about 7.3 meV (see Fig. S-10 in Ref. [50]). This difference indicates that $Ba_I(6d)$-weighted modes are more extended in the crystal than the $Ba_{IX}(12d)$-weighted modes. For Ba sites in Ba_8Si_{46}, the value of β extracted from the *ab initio* potentials are smaller by a factor of 2 to 3 than in $Ba_{24}Si_{100}$ which is in agreement with the absence of a temperature effect on the Ba-weighted phonon energies as seen by INS [16] and discussed previously.

IV. CONCLUSION

This work reveals that the phonon spectrum in the binary $Ba_{24}Si_{100}$ (type-IX clathrate) contains Ba-weighted modes at significantly lower energies than those found in the binary Ba_8Si_{46} (type-I clathrate). The energy downshift of the low-energy optical spectrum is ascribed to the difference in the cage geometry and size. The low-lying optical phonons in $Ba_{24}Si_{100}$ are associated with Ba motions in the open Si_{20} cage (site 12d) along the twofold axis while, in Ba_8Si_{46}, they mostly correspond to Ba motions in the Si_{24} cages (site 6d). Both open Si_{20} and Si_{24} cages are anisotropic with the softest Ba potentials in the direction where the Ba-Si distances

are the highest. The guest potential in the open Si_{20} cage appears much more anisotropic than the one in the Si_{24} cage. Moreover, the calculated $Ba_{IX}(12d)$ potential in the *open* Si_{20} cage exhibits an anharmonicity significantly more pronounced than the one of the $Ba_I(6d)$ in the Si_{24} cage. It corroborates the experimental finding of a detectable softening of the $Ba_{IX}(12d)$-weighted optical phonon energies upon cooling, while no temperature change is identified for the energies of $Ba_I(6d)$-weighted optical phonons

Ab initio calculations in the harmonic approximation show that the $Ba_{IX}(12d)$-weighted modes are characterized by very low values of their PR going down to 0.0365, lower than the PR values in Ba_8Si_{46} and almost similar to the PR of localized modes in disordered systems. Such low values of the PR, obtained in the harmonic calculations, reveal that the associated eigenstates involve only few atoms with nonzero amplitudes in the unit cell. This is corroborated by the fact that the $Ba_{IX}(12d)$-weighted mode energies are very close to the harmonic energies deduced from the quadratic terms of the *ab initio* potential.

In both clathrates, the low-lying Ba-weighted modes result in flat optical bands, which are responsible for a strong bending of the acoustic (transverse and longitudinal) branches and limit their dispersions towards higher energies. In the type-IX clathrate, the $Ba_{IX}(12d)$-weighted phonon band spreads out in the 2.5–4 meV range while, in the type-I, the $Ba_I(6c)$-weighted band is located at higher energies between 7 and 9 meV. The available energy range for acoustic phonon states in $Ba_{24}Si_{100}$ is then shrunk by almost a factor of 2 in comparison to Ba_8Si_{46}, which necessarily impacts the thermal conduction. Indeed, in type-I clathrate, the thermal conductivity is found to depend linearly on the energy of the low-lying guest optical phonon E_{guest} [23]. From the phonon dispersion curves, we have calculated the sound velocity v_s of both type-I Ba_8Si_{46} and type-IX $Ba_{24}Si_{100}$ (see the Supplemental Material for the details) [50,73,74]. In the case of type-I Ba_8Si_{46} and type-IX $Ba_{24}Si_{100}$, the product $E_{guest}.v_s$ is equal to 26 eV m s^{-1} and 12.5 eV m s^{-1}, respectively. If we consider the scaling relation found by Ikeda *et al.* [23], this means that the thermal conductivity in the type-IX clathrate is expected to be two times lower than in type-I clathrate, i.e., about 1 W m^{-1} K^{-1}, which corresponds to an increase in the thermoelectric figure of merit by a factor of 2.

[1] *The Physics and Chemistry of Inorganic Clathrates*, edited by G. S. Nolas, Springer Series in Materials Science (Springer, Berlin, 2014), p. 199.

[2] T. Takabatake, K. Suekuni, T. Nakayama, and E. Kaneshita, Rev. Mod. Phys. **86**, 669 (2014).

[3] M. Christensen, S. Johnsen, and B. B. Iversen, Dalton Trans. **39**, 978 (2010).

[4] J. A Dolyniuk *et al.*, Mater. Sci. Eng. R **108**, 1 (2016).

[5] T. Takabatake, Nano-Cage Structured Materials: Clathrates, in *Thermoelectric Nanomaterials: Materials Design and Applications*, edited by K. Koumoto and T. Mori (Springer-Verlag, Berlin, 2013).

[6] S. Yamanaka, Dalton Trans. **39**, 1901 (2010).

[7] C. H. Lee, H. Yoshizawa, M. A. Avila, I. Hase, K. Kihou, and H. Sato, J. Phys.: Conf. Series **92**, 012169 (2007).

[8] M. Christensen, A. B. Abrahamsen, N. B. Christensen, F. Juranyi, N. H. Andersen, K. Lefmann, J. Andreasson, C. R. H. Bahl, and B. B. Iversen, Nat. Mater. **7**, 811 (2008).

[9] H. Euchner, S. Pailhès, L. T. K. Nguyen, W. Assmus, F. Ritter, A. Haghighirad, Y. Grin, S. Paschen, and M. de Boissieu, Phys. Rev. B **86**, 224303 (2012).

[10] S. Pailhès, H. Euchner, V. M. Giordano, R. Debord, A. Assy, S. Gomés, A. Bosak, D. Machon, S. Paschen, and M. de Boissieu, Phys. Rev. Lett. **113**, 025506 (2014).

[11] P.-F. Lory *et al.*, Nat. Commun. **8**, 491 (2017).

[12] S. Pailhès, V. M. Giordano, P.-F. Lory, M. De Boissieu, H. Euchner, and K. Termendzidis, *Nanostructured Semiconductors: Amorphization and Thermal Properties* (Pan Stanford Publishing Pte. Ltd., Singapore, 2017), Chap. 19.

[13] E. Reny *et al.*, Phys. Rev. B **66**, 014532 (2002).

[14] R. P. Hermann, W. Schweika, O. Leupold, R. Rüffer, G. S. Nolas, F. Grandjean, and G. J. Long, Phys. Rev. B **72**, 174301 (2005).

[15] M. Christensen, F. Juranyi, and B. B. Iversen, Phys. B **385–386**, 505 (2006).

[16] R. Lortz, R. Viennois, A. Petrovic, Y. Wang, P. Toulemonde, C. Meingast, M. M. Koza, H. Mutka, A. Bossak, and A. San Miguel, Phys. Rev. B **77**, 224507 (2008).

[17] M. M. Koza, M. R. Johnson, H. Mutka, M. Rotter, N. Nasir, A. Grytsiv, and P. Rogl, Phys. Rev. B **82**, 214301 (2010).

[18] S. Johnsen, M. Christensen, B. Thomsen, G. K. H. Madsen, and B. B. Iversen, Phys. Rev. B **82**, 184303 (2010).

[19] B. C. Sales, B. C. Chakoumakos, R. Jin, J. R. Thompson, and D. Mandrus, Phys. Rev. B **63**, 245113 (2001).

[20] K. Umeo, M. A. Avila, T. Sakata, K. Suekuni, and T. Takabatake, J. Phys. Soc. Jpn. **74**, 2145 (2005).

[21] M. A. Avila, K. Suekuni, K. Umeo, H. Fukuoka, S. Yamanaka, and T. Takabatake, Phys. Rev. B **74**, 125109 (2006).

[22] K. Suekuni, M. A. Avila, K. Umeo, and T. Takabatake, Phys. Rev. B **75**, 195210 (2007).

[23] M. S. Ikeda, H. Euchner, X. Yan, P. Tomes, A. Prokofiev, L. Prochaska, G. Lientschnig, R. Svarega, S. Hartman, E. Gati, M. Lang, and S. Paschen, Nat. Commun. **10**, 887 (2019).

[24] H. Euchner, S. Pailhès, V. M. Giordano, and M. de Boissieu, Phys. Rev. B **97**, 014304 (2018).

[25] T. Tadano, Y. Gohda, and S. Tsuneyuki, Phys. Rev. Lett. **114**, 095501 (2015).

[26] P. Norouzzadeh, J. S. Krasinski, and T. Tadano, Phys. Rev. B **96**, 245201 (2017).

[27] Q. Xi, Z. Zhang, J. Chen, J. Zhou, T. Nakayama, and B. Li, Phys. Rev. B **96**, 064306 (2017).

[28] Y. Liu, Q. Xi, J. Zhou, T. Nakayama, and B. Li, Phys. Rev. B **93**, 214305 (2016).

[29] T. Tadano and S. Tsuneyuki, Phys. Rev. Lett. **120**, 105901 (2018).

[30] U. Aydemir, C. Candolfi, A. Omerci, H. Borrmann, U. Burkhardt, Y. Oztan, N. Oeschler, M. Baitinger, F. Steglich, and Y. Grin, Inorg. Chem. **51**, 4730 (2012).

[31] K. Momma and F. Izumi, J. Appl. Crystallogr. **44**, 1272 (2011).

[32] H. Fukuoka and S. Yamanaka, J. Organomet. Chem. **611**, 543 (2000).

[33] R. Viennois, P. Toulemonde, C. Paulsen, and A. San Miguel, J. Phys.: Condens. Matter **17**, L311 (2005).

[34] P. Toulemonde, D. Machon, A. San Miguel, and M. Amboage, Phys. Rev. B **83**, 134110 (2011).

[35] W. Carrillo-Cabrera, H. Borrmann, S. Paschen, M. Baenitz, F. Steglich, and Y. Grin, J. Solid State Chem. **178**, 715 (2005).

[36] P. Toulemonde, A. San Miguel, A. Merlen, R. Viennois, S. Le Floch, Ch. Adessi, X. Blase, and J. L. Tholence, J. Phys. Chem. Solids **67**, 1117 (2006).

[37] J. Ollivier and H. Mutka, J. Phys. Soc. Jpn. **80**, SB003 (2008).

[38] R. Viennois, P. Toulemonde, M. Koza, H. Mutka, A. San Miguel, and R. Lortz J. Phys.: Conf. Ser. **92**, 012121 (2007).

[39] M. M. Koza, A. Leithe-Jasper, H. Rosner, W. Schnelle, H. Mutka, M. R. Johnson, and Y. Grin, Phys. Rev. B **89**, 014302 (2014).

[40] M. M. Bredov, B. A. Kotov, N. M. Okuneva, V. S. Oskotskii, and A. L. Shakh-Budagov, Fizika Tverdogo Tela **9**, 287 (1967) [Sov. Phys. Solid State **9**, 214 (1967).

[41] V. S. Oskotskii, Fizika Tverdogo Tela **9**, 550 (1967) [Sov. Phys. Solid State **9**, 420 (1967)].

[42] G. Kresse and D. Joubert, Phys. Rev. B **59**, 1758 (1999).

[43] J. P. Perdew, K. Burke, and M. Ernzerhof, Phys. Rev. Lett. **77**, 3865 (1996).

[44] M. Methfessel and A. T. Paxton, Phys. Rev. B **40**, 3616 (1989).

[45] H. Fukuoka and S. Yamanaka, Inorg. Chem. **39**, 56 (2000).

[46] J. Hafner, J. Comput. Chem. **29**, 2044 (2008).

[47] K. Parlinski, AIP Conf. Proc. **479**, 121 (1999).

[48] M. M. Koza, M. R. Johnson, R. Viennois, H. Mutka, L. Girard, and D. Ravot, Nat. Mater. **7**, 805 (2008).

[49] M. M. Koza, L. Capogna, A. Leithe-Jasper, H. Rosner, W. Schnelle, H. Mutka, M. R. Johnson, C. Ritter, and Y. Grin, Phys. Rev. B **81**, 174302 (2010).

[50] See Supplemental Material at http://link.aps.org/supplemental/10.1103/PhysRevB.101.224302 for the calculations of the atomic potential of silicon in $Ba_{24}Si_{100}$, the calculations of the isotropic atomic displacement parameters of $Ba_{24}Si_{100}$ and Ba_8Si_{46}, the inelastic response of $Ba_{24}Si_{100}$ in the extended energy range, the additional details of the lattice dynamics calculations of $Ba_{24}Si_{100}$ and Ba_8Si_{46}, the elastic constants of $Ba_{24}Si_{100}$ and Ba_8Si_{46} from DFT calculations, the calculations of the volume of the cages of $Ba_{24}Si_{100}$ and Ba_8Si_{46}, and the electronic density of states of $Ba_{24}Si_{100}$ and Ba_8Si_{46}.

[51] Y. Takasu, T. Hasegawa, N. Ogita, M. Udagawa, M. A. Avila, K. Suekuni, and T. Takabatake, Phys. Rev. Lett. **100**, 165503 (2008).

[52] Y. Takasu, T. Hasegawa, N. Ogita, M. Udagawa, M. A. Avila, K. Suekuni, I. Ishii, T. Suzuki, and T. Takabatake, Phys. Rev. B **74**, 174303 (2006).

[53] Y. Takasu, T. Hasegawa, N. Ogita, M. Udagawa, M. A. Avila, K. Suekuni, and T. Takabatake, Phys. Rev. B **82**, 134302 (2010).

[54] H. Fukuoka, J. Kiyoto, and S. Yamanaka, J. Solid State Chem. **175**, 237 (2003).

[55] H. Fukuoka, K. Iwai, S. Yamanaka, H. Abe, K. Yoza, and L. Häming, J. Solid State Chem. **151**, 117 (2000).

[56] W. Carillo-Cabrera, J. Curda, K. Peters, S. Paschen, Yu. Grin, and H. G. von Schnering, Z. Kristallogr. **215**, 321 (2000).

[57] S.-J. Kim, S. Hu, C. Uher, T. Hogan, B. Huang, J. D. Corbett, and M. G. Kanatzidis, J. Solid State Chem. **153**, 321 (2000).

[58] N. L. Okamura, J.-H. Kim, K. Tanaka, and H. Inui, Acta Mater. **54**, 5519 (2006).

[59] T. F. Fässler and C. Kronseder, Z. Anorg. Allg. Chem. **624**, 561 (1998).

[60] H. G. von Schnering, A. Zürn, J.-H. Chang, M. Baitinger, and Y. Grin, Z. Anorg. Allg. Chem. **633**, 1147 (2007).

[61] J. S. Tse, T. Iitaka, and K. Parlinski, Europhys. Lett. **75**, 153 (2006).

[62] H. Shimizu, T. Kume, T. Kuroda, S. Sasaki, H. Fukuoka, and S. Yamanaka, Phys. Rev. B **71**, 094108 (2005).

[63] A. Moll, M. Beaudhuin, V. Legrand, R. Debord, S. Pailhès, R. Viennois, and N. Fréty, Mater. Lett. **187**, 1 (2017).

[64] G. Lucazeau, J. Raman Spectroscop. **34**, 478, (2003).

[65] T. Tadano and S. Tsuneyuki. J. Phys. Soc. Jpn. **87**, 041015 (2018).

[66] T. Kume, H. Fukuoka, T. Koda, S. Sasaki, H. Shimizu, and S. Yamanaka, Phys. Rev. Lett. **90**, 155503 (2003).

[67] T. Mori *et al.*, Phys. Rev. B **79**, 212301 (2009).

[68] T. Dahm and K. Ueda, Phys. Rev. Lett. **99**, 187003 (2007).

[69] H. Mutka, M. M. Koza, M. R. Johnson, Z. Hiroi, J.-I. Yamaura, and Y. Nagao, Phys. Rev. B **78**, 104307 (2008).

[70] Y. Bouyrie *et al.*, Phys. Chem. Chem. Phys. **17**, 19751 (2015).

[71] M. M. Koza, H. Mutka, Y. Okamoto, J.-I. Yamaura, and Z. Hiroi, Phys. Chem. Chem. Phys. **17**, 24837 (2015).

[72] M. M. Koza, A. Leithe-Jasper, H. Rosner, W. Schnelle, H. Mutka, M. R. Johnson, M. Krisch, L. Capogna, and Y. Grin, Phys. Rev. B **84**, 014306 (2011).

[73] Z.-J. Wu, E.-J. Zhao, H.-P. Xiang, X.-F. Hao, X.-J. Liu, and J. Meng, Phys. Rev. B **76**, 054115 (2007).

[74] Y. Ding and B. Xiao, Comp. Mater. Sci. **82**, 202 (2014).